

# Chapter 7

## Films of a Non-ionic ImTp Molecule: Effect of Ionic Polar Group on LB Deposition

### 7.1 Introduction

Langmuir-Blodgett (LB) technique is widely used in the fabrication of ultrathin organized films with specific properties and functionality. The inherent theoretical interest and potential applicability have forced intensive investigations in the preparation, characterization and utilization of nanostructured films with controlled structure, composition and thickness [1]. It is known that formation of LB films are very sensitive to experimental conditions like subphase composition, properties of the floating monolayer, surface pressure and rate of deposition [2]. The deposition of monolayer on a substrate is accompanied by complicated physical and chemical interactions between the substrate and the monolayer near the three-phase contact line. Molecular interactions and reorganization [3], hydrodynamic processes [4], phase transitions [5], electrostatic interactions [6], monolayer ionization, and counterion binding [7] play crucial roles between the substrate and the monolayer. These processes influence the monolayer transfer ratio, structure and morphology of the LB films. An understanding of the processes during the monolayer deposition is extremely important to control and modify the properties of the LB films.

In case of charged Langmuir monolayer, the deposition process becomes even more complicated [8]. Here, electrostatic double layer interactions are strongly affected by the electrolyte concentration in the subphase. At dynamic conditions, the ion concentration within the overlapping diffuse layers deviates from equilibrium. These processes play a decisive role in the formation and stability of LB films of charged monolayers. In literature, the most widely studied ionizable

Langmuir monolayers include the fatty acids and fatty amines [9]. These molecules get ionized at the interface which can chemically interact with the ions in the subphase to form surface active complexes. Their monolayer properties are markedly different from those of the un-ionized fatty molecules. Mahnke et al. observed meniscus oscillations (so-called “slip-stick” behavior) during deposition of arachidic acid monolayers [10]. Kovalchuk et al. observed stripe pattern in the atomic force microscope images of LB films of cadmium arachidate arising due to meniscus instability [11]. Analogous stripe patterns were also observed for phospholipid (DPPC) monolayer LB films on silicon surface [12].

In the previous chapters of this thesis, we have dealt with molecules which are ionic discotic amphiphiles. We have studied their organization at the air-water (A-W) as well as air-solid interfaces. We observed that for all the ionic discotic monolayers, multilayer formation by LB technique was difficult. On adding small amount of DNA in the subphase, the LB transfer efficiency increased drastically leading to the formation of stable multilayers [13]. In this chapter, we show the monolayer formation of a non-ionic discotic molecule, *viz.*, imidazole tethered with hexaalkoxytriphenylene (N-ImTp) at the A-W interface. We compare the monolayer properties of N-ImTp with that of its ionic analog, *viz.*, imidazolium tethered with hexaalkoxytriphenylene with bromine counterion (ImTp) presented in Chapter 2. We find that the N-ImTp monolayer exhibits lower limiting area and higher compressional elastic modulus as compared to its ionic analog. Interestingly, the LB film deposition of N-ImTp monolayer was found to be efficient over several layers unlike that of the ImTp monolayer.

## 7.2 Experiment

The material N-ImTp was synthesized in the chemistry laboratory of our institute by Prof. Sandeep Kumar and Santanu Kumar Pal. The material was purified by repeated recrystallizations with diethyl ether and characterized by  $^1\text{H}$  NMR,  $^{13}\text{C}$  NMR, IR, UV spectroscopy and elemental analysis which indicated high purity (99%) of the material. The thermotropic liquid crystalline properties of the material was investigated by polarizing optical microscopy and differential scanning calorimetry. This material does not show any liquid crystalline phase. On heating, the N-ImTp material

directly goes from crystalline phase to isotropic liquid phase at 50°C.

We have carried out the surface manometry studies in a LB trough. The subphase used was ultrapure deionized water. The stock solution was prepared with HPLC grade chloroform at a concentration of 0.1 mg/ml. The monolayer compression speed was 10 cm<sup>2</sup>/min. Brewster angle microscope (BAM) was used to observe the film morphology at the air-water interface. LB technique was used to transfer the film from the air-water (A-W) interface onto polished silicon wafers. We have used both hydrophilic and hydrophobic silicon substrates for the LB deposition. The details of the substrate preparation are presented in Chapter 2. The dipping speed in the LB deposition process was maintained at 2 mm/min. An atomic force microscope (AFM) was employed to study the film topography at the air-solid interface. The details of these experimental techniques are presented in Chapter 1.

## 7.3 Results and Discussion

### 7.3.1 Surface Manometry

The surface pressure ( $\pi$ ) - area per molecule ( $A_m$ ) isotherm of N-ImTp molecule on ultrapure deionized water subphase is shown in Figure 7.1. We find that the surface pressure starts increasing around an  $A_m$  of 2.0 nm<sup>2</sup>/molecule which is followed by a steep rise, until it reaches collapse at about 0.66 nm<sup>2</sup>/molecule. The isotherm shows a limiting area ( $A_o$ ) of 1 nm<sup>2</sup>/molecule and a collapse pressure of about 31.4 mN/m. This  $A_o$  value is much less compared to the  $A_o$  value of ImTp monolayer (1.4 nm<sup>2</sup>/molecule) [14]. This indicates that the absence of direct electrostatic repulsion in the N-ImTp monolayer facilitates close packing of the molecules leading to a lower  $A_o$  value [9]. In addition, comparing with the molecular dimension (shown in Chapter 2), the  $A_o$  value of 1 nm<sup>2</sup>/molecule suggests an edge-on arrangement of the molecules in the N-ImTp monolayer at the A-W interface.

The  $\pi$ - $A_m$  isotherm of N-ImTp monolayer in the compression and expansion cycles from the monolayer state to the collapsed state is shown in Figure 7.2. We observed negligible hysteresis in the isotherm cycles. This indicates that the N-ImTp monolayer exhibits reversible collapse similar to that of the ionic discotic monolayers presented in the previous chapters.

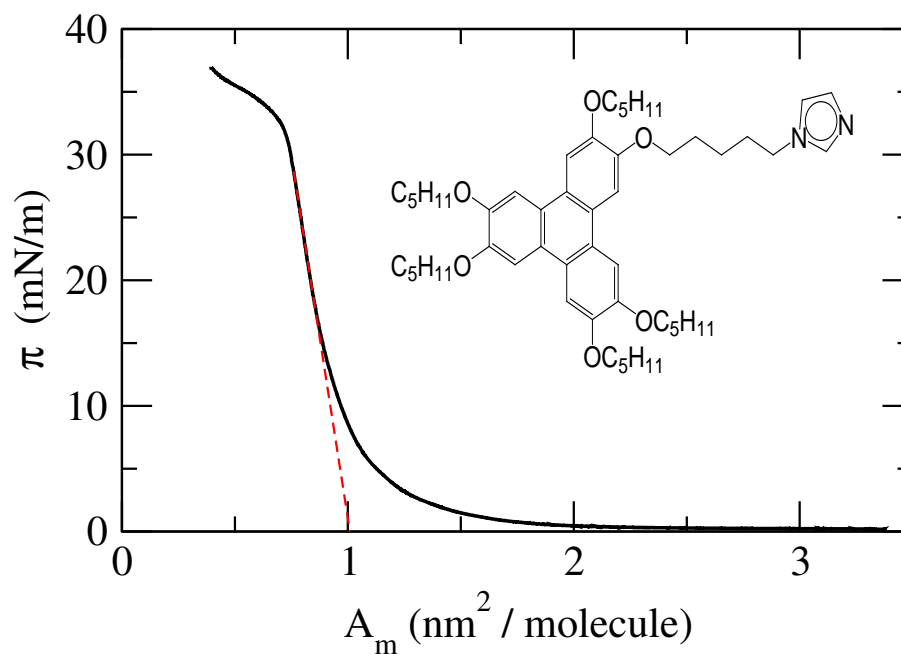


Figure 7.1: The surface pressure ( $\pi$ ) - area per molecule ( $A_m$ ) isotherm of N-ImTp monolayer on ultrapure water subphase. The dashed-line is drawn to obtain the limiting area per molecule.

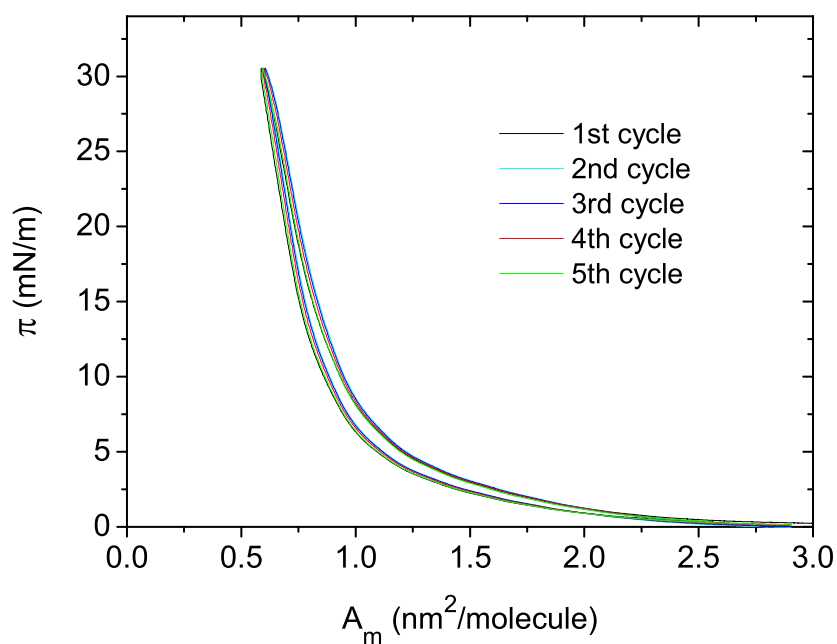


Figure 7.2: The  $\pi - A_m$  isocycles obtained by compression and expansion of N-ImTp monolayer at the air-water interface, showing reversibility from the collapsed state to the monolayer state with negligible hysteresis.

The variation of compressional elastic modulus ( $|E|$ ) with  $A_m$  for N-ImTp monolayer at the A-W interface is shown in Figure 7.3. Here,  $|E|$  is given by  $A_m (d\pi/dA_m)$ , which can be calculated from the  $\pi - A_m$  isotherm. We find a maximum  $|E|$  value of 76 mN/m for the N-ImTp monolayer. This value is about 29% higher than the  $|E|$  value attained by the ImTp monolayer (53.9 mN/m) [14]. This provides further evidence for a better packing of molecules in the N-ImTp monolayer compared to its ionic analog. It should be noted that, in case of an ionic discotic monolayer, there is a competition between two types of interaction: (i) the  $\pi$ - $\pi$  stacking interaction between the discotic cores that favors close packing of molecules in the monolayer, and (ii) the electrostatic repulsion between the molecules that opposes this close packing. Therefore, for an ionic discotic monolayer, the close packing of molecules is not much favored, unlike that of a non-ionic discotic monolayer where the  $\pi$ - $\pi$  stacking interaction is dominant.

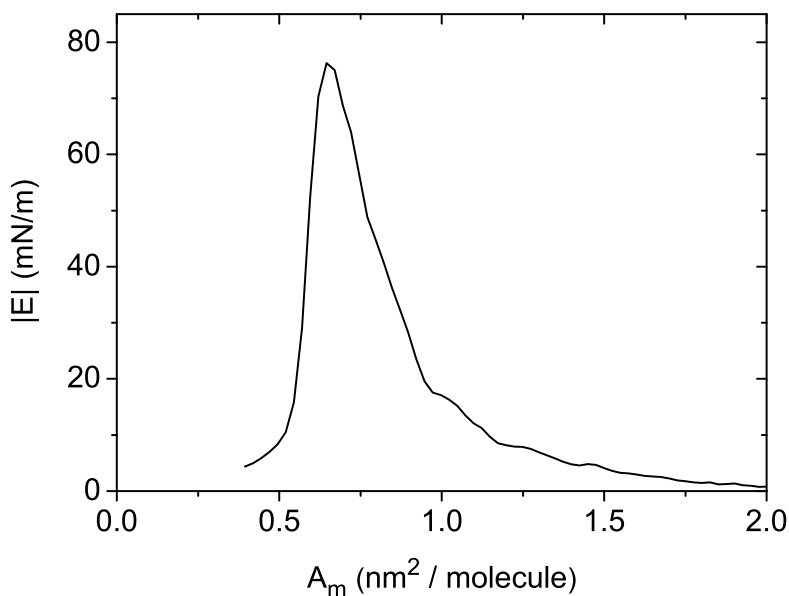


Figure 7.3: Variation of compressional elastic modulus ( $|E|$ ) with area per molecule ( $A_m$ ) for N-ImTp monolayer at the air-water interface.

### 7.3.2 Brewster Angle Microscopy

The morphology of the N-ImTp film at the air-water interface was observed under a BAM during compression and expansion of the monolayer. Figure 7.4 shows BAM images of the N-ImTp

monolayer at different  $A_m$  values. At large  $A_m$ , the monolayer appeared uniform and its brightness increased upon compression (Figure 7.4(b)). We find three-dimensional (3D) crystalline domains developing over the uniform phase at an  $A_m$  of around  $0.70 \text{ nm}^2/\text{molecule}$  indicating the onset of collapse (Figure 7.4(c)). Upon further compression, the monolayer fully transformed to crystalline domains (Figure 7.4(d)). These crystalline domains reverted back to the uniform monolayer state upon expansion of the film. This confirms the reversibility of the N-ImTp film from the collapsed state to the monolayer state. This behavior is similar to that of the ionic discotic monolayers presented in the previous chapters.

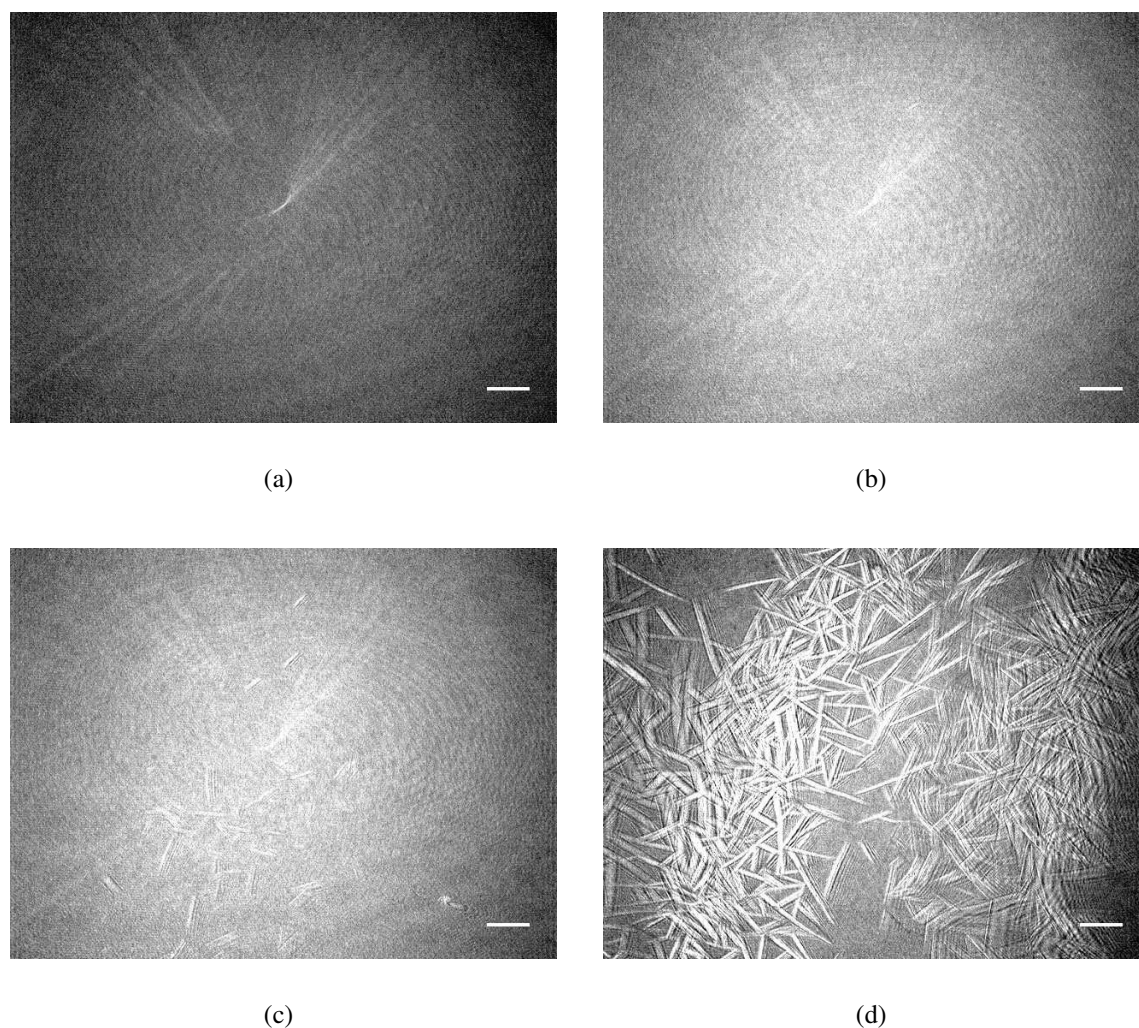


Figure 7.4: Brewster angle microscope images of N-ImTp monolayer at the air-water interface. (a) Clean water surface. (b) Condensed monolayer film at  $A_m = 0.90 \text{ nm}^2/\text{molecule}$ . (c) Onset of 3D crystals at  $A_m = 0.70 \text{ nm}^2/\text{molecule}$  indicating the collapsed state. (d) Collapsed state at  $A_m = 0.64 \text{ nm}^2/\text{molecule}$ . The scale bar in each image represents  $500 \mu\text{m}$ .

### 7.3.3 Atomic Force Microscopy

We have transferred the N-ImTp monolayer from the air-water interface to silicon substrates by LB technique. Figure 7.5(a) shows the LB film of the N-ImTp with single layer transferred onto hydrophilic silicon substrate at a target surface pressure ( $\pi_t$ ) of 27 mN/m. The film surface was uniform and the film height was about 2 nm with respect to the substrate. This value corresponds to the estimated height of the molecules arranged in an edge-on configuration (Chapter 2). The LB film of N-ImTp with two layers on hydrophobic silicon substrate at a  $\pi_t$  of 27 mN/m is shown in Figure 7.5(b). The film height for two layers was about 4 nm with respect to the substrate. This value corresponds to the estimated height of the molecules in an edge-on configuration with two layers.

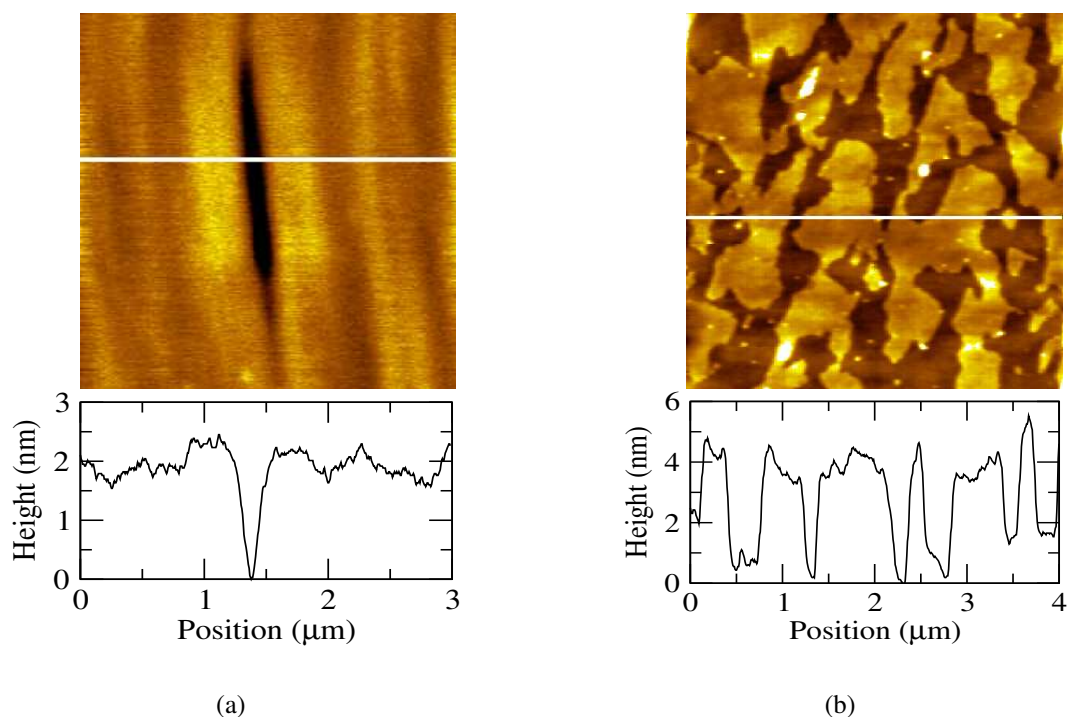


Figure 7.5: AFM topography images of N-ImTp LB film with (a) 1 layer on hydrophilic silicon substrate, and (b) 2 layers on hydrophobic silicon substrate. The respective height profiles corresponding to the lines drawn on the images are shown below.

We have formed multilayers of N-ImTp film on silicon substrates. Figure 7.6 shows AFM topography images of N-ImTp LB film with 20 layers on hydrophobic silicon substrate transferred at a  $\pi_t$  of 27 mN/m. The film morphology showed voids of various depth. The maximum film

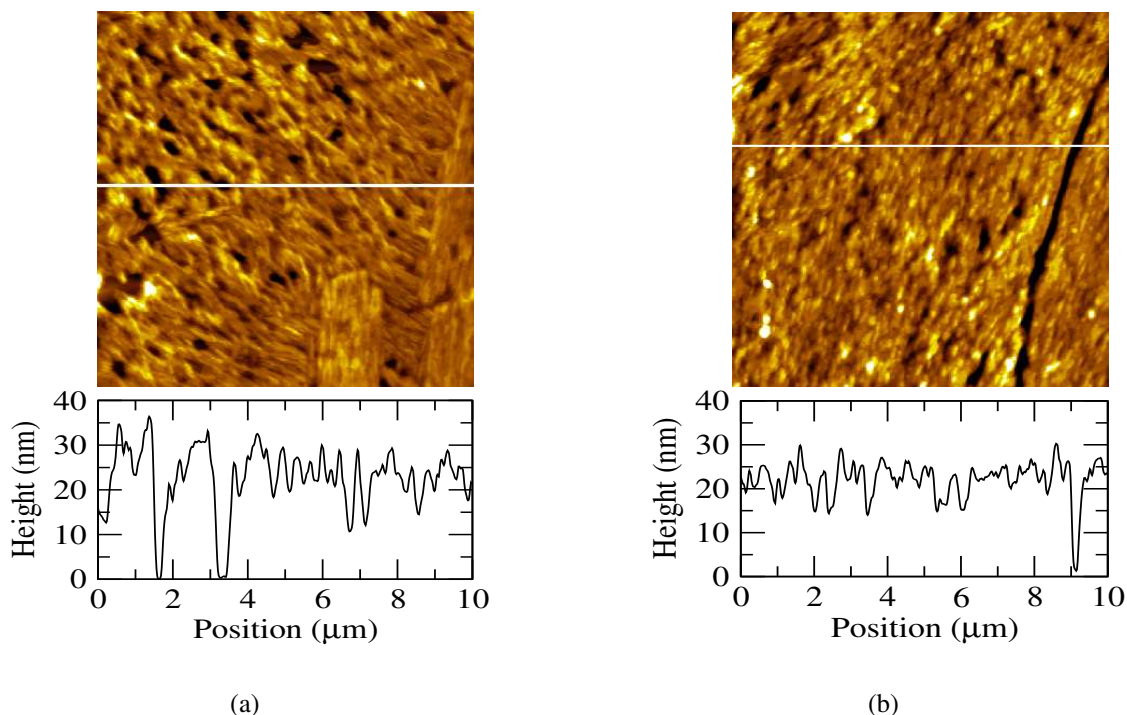
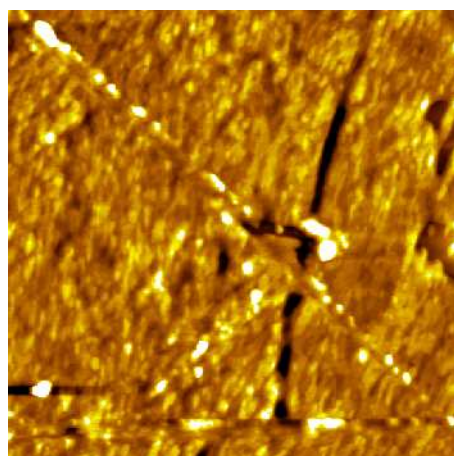
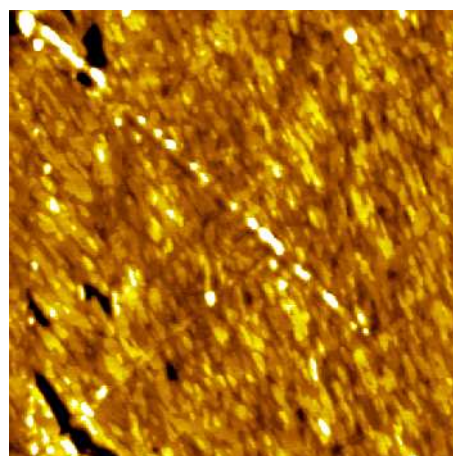


Figure 7.6: AFM topography images of N-ImTp film with 20 layers on hydrophobic silicon substrate. (a) Region 1. (b) Region 2. The respective height profiles corresponding to the lines drawn on the images are shown below.

height obtained with respect to these voids was in the range of 20 to 25 nm. To find the actual film height, we have tried scratching the film with AFM tip. However, the films could not be scratched successfully even with a tip force of the order of 150 nN. A force more than this would damage the tip even before the completion of scratching. The images with scratch on the film surface obtained on various regions with different forces are shown in Figure 7.7. However, we have tried an alternate method to estimate the height of this film. We find that the film exhibited voids of different depths. We have shown in Chapter 4 that the phase imaging can distinguish surfaces with different elastic moduli. The surface covered with film and the bare silicon substrate will have different moduli of elasticity. Therefore, it should be possible to distinguish the exposed substrate and the film covered surface under hard tapping conditions. Figure 7.8 shows AFM topography image of this film and its simultaneously acquired phase image. As can be seen from the phase image, some of these voids appeared very bright. The film heights corresponding to these voids were highest compared to rest of the film. Hence, these voids may correspond to the exposed silicon substrate. The height of this film with respect to such a void was found to be about 22 nm.

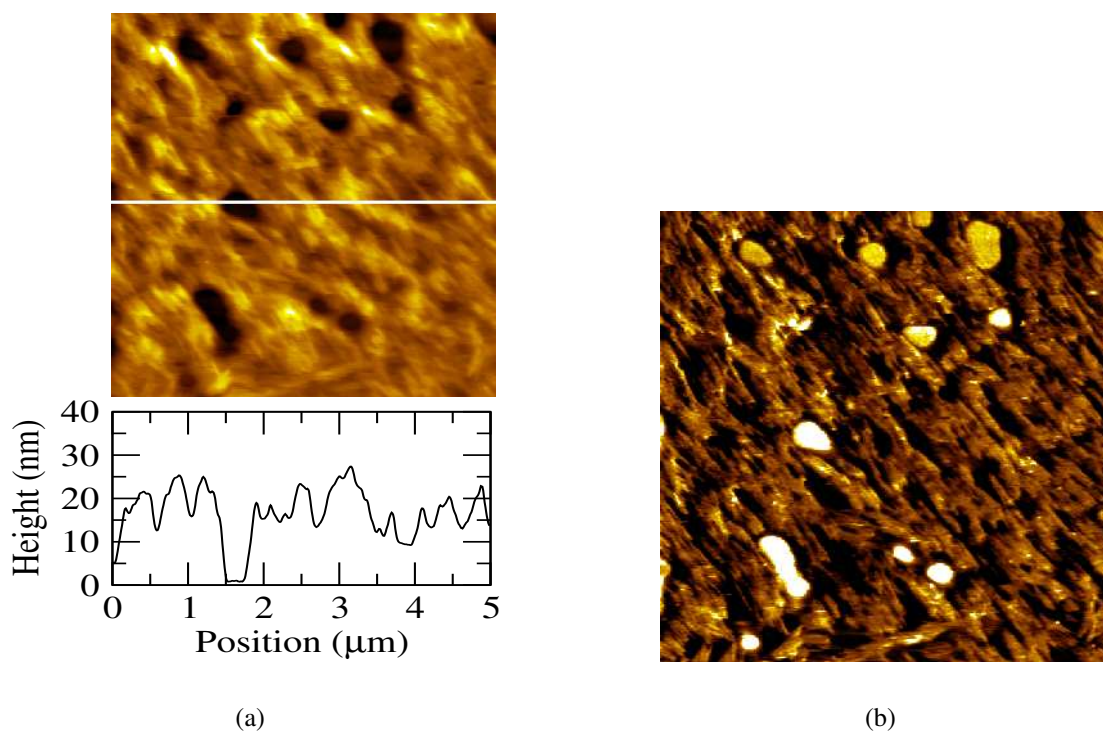


(a)



(b)

Figure 7.7: AFM topography images of N-ImTp LB film with 20 layers on hydrophobic silicon substrate showing scratch impression. (a) Region 1, with a tip force of 100 nN. (b) Region 2, with a tip force of 150 nN.



(a)

(b)

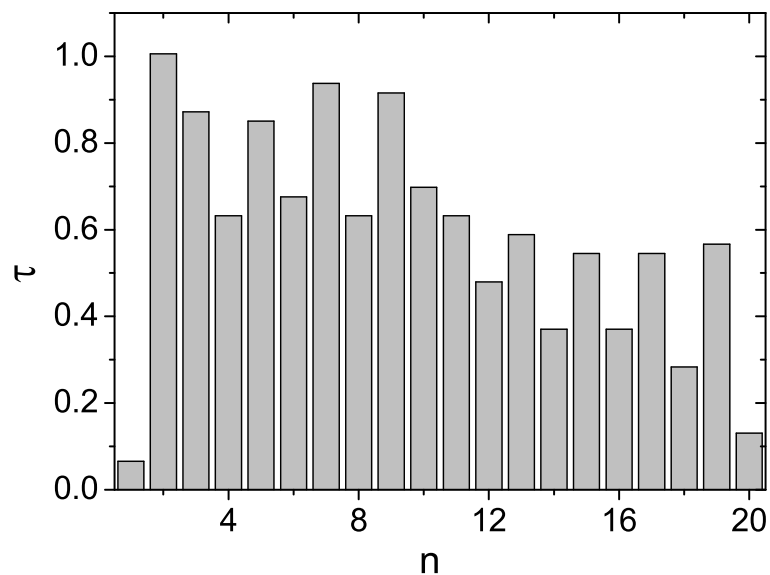
Figure 7.8: AFM images of N-ImTp film with 20 layers on hydrophobic silicon substrate. (a) Topography image. The height profile corresponding to the line drawn on the image is shown below. (b) Phase image revealing contrast between the film and the exposed silicon substrate (voids).

We find that, for N-ImTp monolayer, we could form multilayer with as many as 20 layers, whereas for the ImTp monolayer, it was not possible to transfer more than two layers. This clearly indicates the effect of ionic polar group on the LB deposition process. In the next section, we present the transfer ratio data of these films and discuss briefly the interactions that govern the LB deposition of a charged Langmuir monolayer.

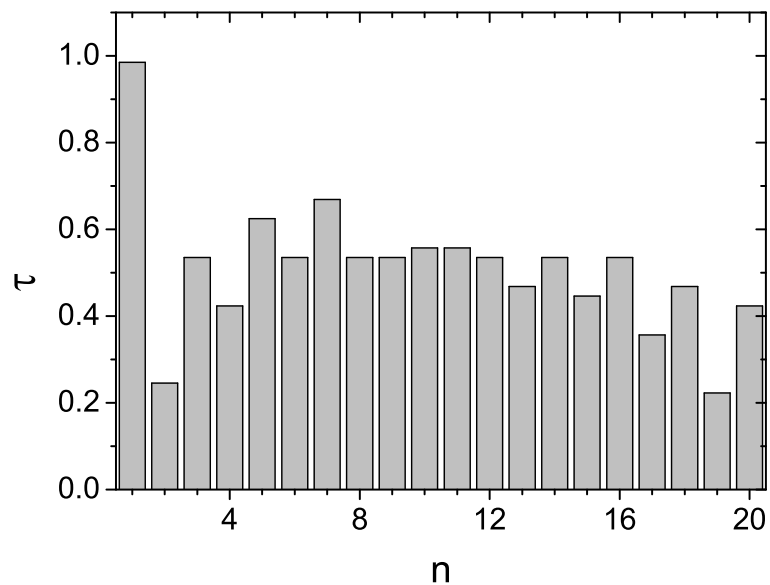
### **7.3.4 Transfer Ratio: Effect of Ionic Polar Head Group on LB Deposition**

The transfer ratio ( $\tau$ ) is defined as the ratio of “the decrease in Langmuir monolayer surface area” to “the total surface area of the substrate to be coated”. A  $\tau$  of unity is indicative of good deposition. The transfer ratio ( $\tau$ ) as a function of number of layers ( $n$ ) of LB deposition for the N-ImTp monolayer is shown in Figure 7.9. The film was transferred at a target surface pressure of 27 mN/m and with a dipping speed of 2 mm/min. Figure 7.9(a) shows the  $\tau$  versus  $n$  data for the film transferred onto hydrophilic silicon substrate and Figure 7.9(b) shows similar data for hydrophobic silicon substrate. We would like to mention that for hydrophilic substrate, the first downstroke does not coat a monolayer because the hydrophilic surface faces the hydrophobic parts of the amphiphiles during the first downstroke [1]. However, it can be seen that the transfer ratio is about unity for the first upstroke of the hydrophilic silicon substrate (Figure 7.9(a)). In the case of hydrophobic silicon substrate (Figure 7.9(b)), the transfer ratio is about unity for the first downstroke of the substrate. For the subsequent strokes of film deposition, the  $\tau$  value was found to decrease slightly in both the cases. However, the efficiency of transfer was observed to be more than 50 % even upto 12 layers.

We have also transferred the ImTp monolayer onto silicon substrates and measured the transfer ratio. Figure 7.10 shows the  $\tau$  versus  $n$  data for the film transferred at a target surface pressure of 35 mN/m and a dipping speed of 2 mm/min. The transfer ratio data for the film transferred on hydrophilic silicon substrate is shown in Figure 7.10(a) and similar data for hydrophobic silicon substrate is shown in Figure 7.10(b). We find that the transfer ratio is about unity for the first two layers of deposition on the hydrophilic silicon substrate (Figure 7.10(a)). For the successive cycles (i.e., one downstroke and one upstroke) of deposition, we find desorption in every upstroke and adsorption in every downstroke. Similar behavior was also observed for the film deposition on a

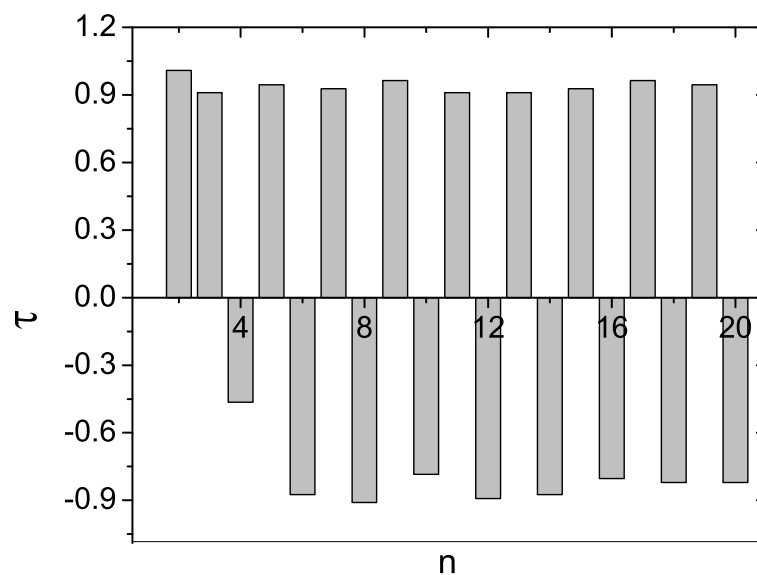


(a)

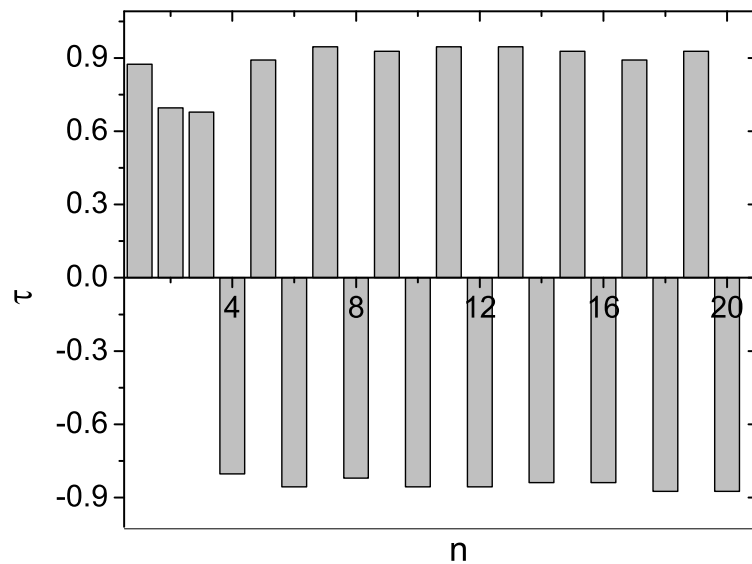


(b)

Figure 7.9: Transfer ratio ( $\tau$ ) as a function of number of layers ( $n$ ) of LB film deposition for N-ImTp on (a) hydrophilic silicon substrate, and (b) hydrophobic silicon substrate. The film transfer was carried out at a target surface pressure of 27 mN/m and a dipping speed of 2 mm/min.



(a)



(b)

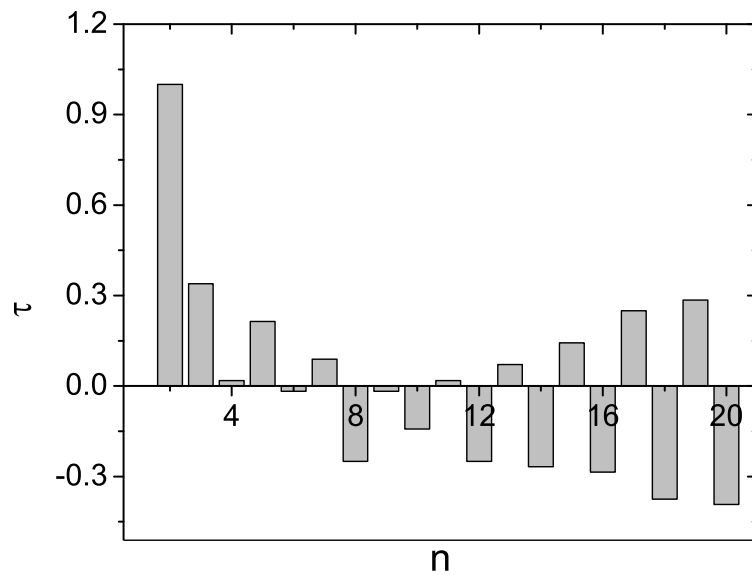
Figure 7.10: Transfer ratio ( $\tau$ ) as a function of number of layers ( $n$ ) of LB film deposition for ImTp on (a) hydrophilic silicon substrate, and (b) hydrophobic silicon substrate. The film transfer was carried out at a target surface pressure of 35 mN/m and a dipping speed of 2 mm/min.

hydrophobic silicon substrate (Figure 7.10(b)).

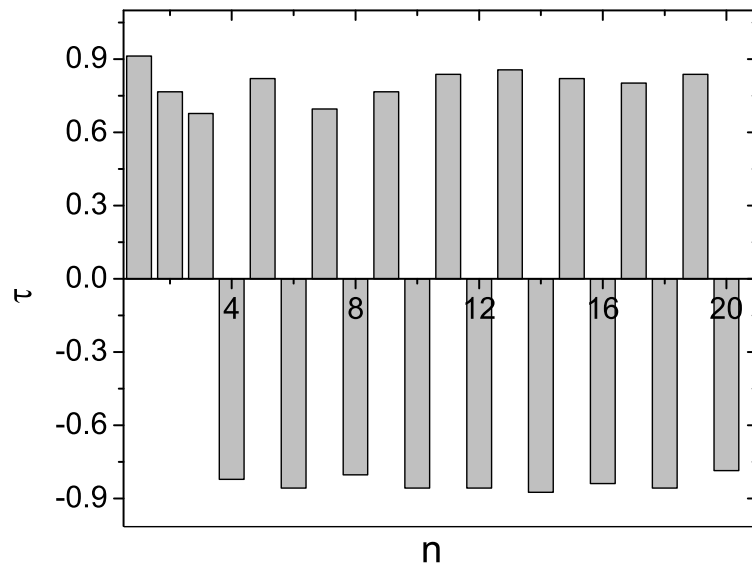
In addition, we have shown the transfer ratio data for the PyTp monolayer in Figure 7.11(a). The film was transferred at a target surface pressure of 35 mN/m and with a dipping speed of 2 mm/min. The film showed a transfer ratio of about unity only for the first upstroke on hydrophilic silicon substrate (Figure 7.11(a)). For the successive deposition cycles, it showed poor  $\tau$  value accompanied by desorption and adsorption in the alternate strokes. On hydrophobic silicon substrate, the film showed efficient transfer only up to the first three layers (Figure 7.11(b)), followed by alternate desorption and adsorption by almost equal amount in the subsequent strokes of deposition.

It can be seen that the transfer of film onto substrate was quite efficient over several layers in the case of the N-ImTp monolayer. This leads to the formation of stable multilayers on a substrate. The transfer efficiency was strikingly different for the case of both the ImTp monolayer and the PyTp monolayer. For both the cases, the film transfer showed alternate adsorption and desorption after the first few layers. Therefore, it was not possible to make a multilayer of the ionic discotic monolayers on a substrate. This suggests that the presence of ionic polar head group prevents efficient transfer. In literature, it is known that the deposition of charged Langmuir monolayer involves complicated physical and chemical processes between the monolayer and the substrate surface [8]. An understanding of these processes is of great importance to control the LB film deposition. In the following, we discuss briefly the important processes that occur during the transfer of a charged Langmuir monolayer.

A charged monolayer at the air-water interface and the adjacent diffuse layer of counterions in the subphase form a totally electro-neutral electric double layer (DL). Here, the interfacial charge of the ionized surface groups is completely compensated by the opposite charge which is spread out within the diffuse layer [15]. In the electric double layer, the positive and negative charges are macroscopically separated. The mean separation of the charges is called the Debye length. For the typical conditions of LB deposition, the Debye length is estimated to be in the order of 10 nm [8]. During Langmuir monolayer deposition, one deals in the vicinity of the three-phase contact line. Close to the three-phase contact line, the electric double layer, which is formed at the air-water interface, overlaps with the double layer at the solid-water interface. The schematic representation



(a)



(b)

Figure 7.11: Transfer ratio ( $\tau$ ) as a function of number of layers ( $n$ ) of LB film deposition for PyTp on (a) hydrophilic silicon substrate, and (b) hydrophobic silicon substrate. The film transfer was carried out at a target surface pressure of 35 mN/m and a dipping speed of 2 mm/min.

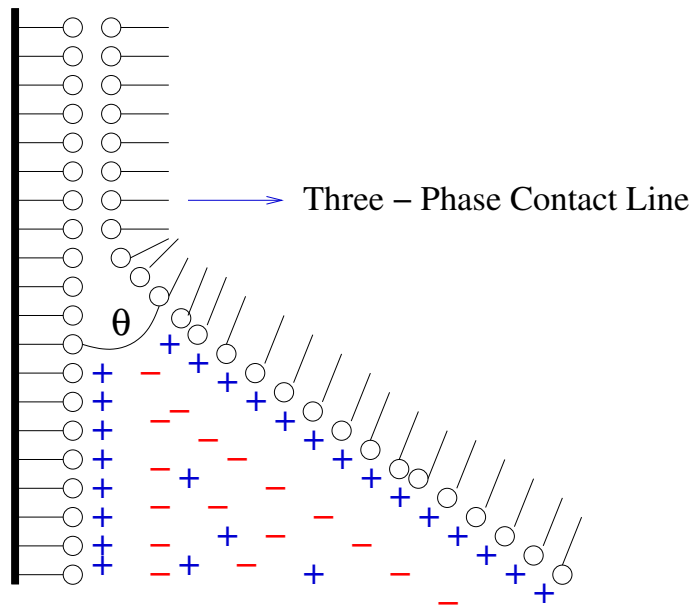


Figure 7.12: Schematic diagram of diffuse double layer overlapping in the meniscus region during the upstroke deposition of a charged Langmuir monolayer (Y-type LB deposition).  $\theta$  is the dynamic contact angle.

of the diffuse double layer overlapping in the meniscus region is shown in Figure 7.12.

The overlapping of DL causes deficiency of counterions in the meniscus region [16]. An important point to note is that a deposited LB film from a charged monolayer is actually electro-neutral. During the deposition process, the monolayer binds counterions from the subphase, which compensate the surface charge before its deposition to the solid substrate. For a complete compensation, all counterions within the diffuse layers should move with the same velocity as the charged surfaces. The convective flux of the counterions produced by the substrate motion is not sufficient to compensate the flux of the surface charges. This takes place since only those parts of the diffuse layers which are adjacent to the surfaces can move with the same velocity as that of the surfaces in the direction of the contact line. The more distant parts of the diffuse layers move with smaller velocities or even in the opposite direction because of the circular structure of the convective flow in the solution, produced by the surfaces. The schematic drawing of the convective flow in the vicinity of three-phase contact line is shown in Figure 7.13. The back flow of the subphase expelled from the three-phase contact line hinders the transfer of the counterions to the region of strong overlap of the diffuse layers [11]. Therefore, a deficit of the counterions is produced near the three-phase contact line.

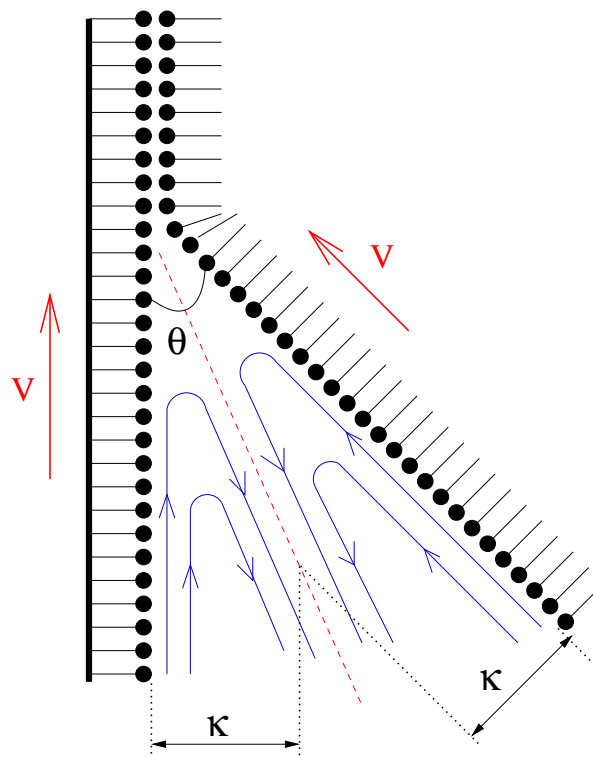


Figure 7.13: Schematic diagram of convective flow in vicinity of the three-phase contact line.  $V$  is the velocity of the surface motion,  $\theta$  is the dynamic contact angle, and  $\kappa$  is the thickness of the diffuse electric double layer (the Debye length).

The electric double layer overlaps in the same region where convective flow is induced by the moving surfaces. This generates non-uniform electric, concentration and hydrodynamic velocity fields [17]. Consequently, a local redistribution of ions occurs in the meniscus region. Such changes of the DL properties under dynamic conditions is typical for electrode and membrane systems and is known as concentration polarization effect [18, 19]. The concentration polarization leads to the decrease of equilibrium contact angle. The contact angle formed between the substrate surface and the floating monolayer during the withdrawal plays a crucial role for the LB-deposition process. It is well known that a successful deposition is observed at large contact angles (“zipper angle” according to Langmuir [20]), whereas, at zero contact angle, entrainment of the water film happens which does not admit multilayer formation. When the withdrawal speed exceeds a critical value, the contact angle spontaneously decreases down to zero. This causes meniscus instability, thereby disrupting the film deposition. In literature, such effects were experimentally observed for the deposition of arachidic acid monolayer and arachidic salt monolayer under various concentra-

tions of counterions in the subphase [10, 11].

We find that, on spreading the ionic discotic molecules at the air-water interface, the small  $\text{Br}^-$  counterions dissolve into the subphase due to the dissociation of the ionic groups. The presence of these  $\text{Br}^-$  counterions in the subphase and the positively charged discotic monolayer at the surface form an electric double layer at the air-water interface. These  $\text{Br}^-$  counterions might not be sufficient enough to compensate the charge of the monolayer during deposition. It is quite possible that concentration polarization would have developed leading to meniscus instability, thereby disrupting the multilayer formation by LB method. On contrary, addition of small amount of DNA ( $\sim 10^{-8}$  M concentration) in the subphase suppresses the concentration polarization effect, thereby facilitating stable multilayer formation. This is evident from the high transfer efficiency ( $\tau \sim 1$ ) observed for the LB deposition of the discotic-DNA complex films presented in Chapter 3 and Chapter 6. We would like to mention that van der Waals forces also play significant role in the adhesion of monolayers, but for the charged monolayer deposition, its contribution is much smaller than the double layer repulsive contribution.

However, DNA is a polyelectrolyte [21]. Its behavior in the solution and its interaction with monolayer at the interface is fairly complex. To understand the LB deposition process of charged discotic monolayers, it would be interesting to put some ionic strength in the subphase by adding simple salts like NaBr or NaCl. A detailed experimental study on the effect of various counterion concentration in the LB film deposition of charged discotic monolayer can be an interesting subject for future research as an extension of this work.

## 7.4 Conclusions

The N-ImTp molecule forms a stable monolayer at the air-water interface. As compared to the monolayer of ImTp (Chapter 2), the N-ImTp monolayer exhibited decreased limiting area and increased compressional elastic modulus. This indicates a better packing of molecules in the N-ImTp monolayer due to the absence of electrostatic repulsion. Interestingly, the transfer of the N-ImTp monolayer to the solid substrate by Langmuir-Blodgett technique showed a markedly different behavior. It was possible to build multilayer of N-ImTp film containing as many as 20 layers with good efficiency. On contrary, its ionic analogs (ImTp and PyTp) could not form multilayers because of alternate desorption and adsorption over the successive strokes of LB deposition. This can be attributed to the fact that concentration polarization inevitably develops in the meniscus region during the deposition of charged monolayers, which causes meniscus instability, thereby disrupting the multilayer formation. Such effects are absent in the case of the N-ImTp monolayer. Therefore, multilayers of N-ImTp monolayer could be formed successfully.

# Bibliography

- [1] G. Roberts, *Langmuir-Blodgett Films*, Plenum Press: New York, 1990.
- [2] D. K. Schwartz, *Surface Science Reports* **27**, 241 (1997).
- [3] R. Aveyard, B. P. Blinks, P. D. I. Fletcher, and X. Ye, *Thin Solid Films* **210/211**, 36 (1992).
- [4] M. Elena Diaz and R. L. Cerro, *Thin Solid Films* **460**, 274 (2004).
- [5] K. Spratte, L. F. Chi, and H. Riegler, *Europhys Lett* **25**, 211 (1994).
- [6] T. Chou, *Phys. Rev. Lett.* **87**, 106101 (2001).
- [7] J. G. Petrov, H. Kuhn, and D. Mobius, *J. Colloid Interface Sci.* **73**, 66 (1980).
- [8] V. I. Kovalchuk and D. Vollhardt, *Adv. Colloid Interface Sci.* **114-115**, 267 (2005).
- [9] G. L. Gaines Jr., *Insoluble Monolayers at Liquid Gas Interface*, Interscience: New York, (1966).
- [10] J. Mahnke, D. Vollhardt, K. W. Stockelhuber, K. Meine, and H. J. Schulze, *Langmuir* **15**, 8220 (1999).
- [11] V. I. Kovalchuk, M. P. Bondarenko, E. K. Zholkovskiy, and D. Vollhardt, *J. Phys. Chem. B* **107**, 3486 (2003).
- [12] H. Riegler and K. Graf, *Colloids Surf. A* **131**, 215 (1998).
- [13] Alpana Nayak and K. A. Suresh, *J. Phys. Chem. B* **112**, 2930, (2008).
- [14] Alpana Nayak, K. A. Suresh, Santanu Kumar Pal, and Sandeep Kumar, *J. Phys. Chem. B* **111**, 11157 (2007).

- [15] J. N. Israelachvili, *Intermolecular and Surface Forces*, Academic Press:London, 1992.
- [16] V. I. Kovalchuk, E. K. Zholkovskiy, N. P. Bondarenko, and D. Vollhardt, *J. Phys. Chem. B* **105**, 9254 (2001).
- [17] J. G. Petrov and P. G. Petrov, *Langmuir* **14**, 2490 (1998).
- [18] S. S. Dukhin, *Adv Colloid Interface Sci.* **44**, 1 (1993).
- [19] N. Lakshminarayanaiah, *Transport Phenomena in Membranes*, New York: Academic Press, 1969.
- [20] I. Langmuir, *Science* **87**, 493 (1938).
- [21] T. Ohnishi, *Biophys. J.* **3**, 459 (1963).